PPPL-2582

UC-420,426

PPPL-2582

PITCH ANGLE RESOLVED MEASUREMENTS OF ESCAPING CHARGED FUSION PRODUCTS IN TFTR

By

S.J. Zweben

JANUARY 1989

PLASMA
PHYSICS
LABORATORY

PPPL--2582

DE89 006878

Pitch Angle Resolved Measurements of Escaping Charged Fusion Products in TFTR

S. J. Zweben

Princeton Plasma Physics Laboratory, Princeton University

Princeton, N.J. 08543

ABSTRACT

Measurements of the flux of charged fusion products escaping from the TFTR plasma have been made with a new type of detector which can resolve the particle flux vs. pitch angle, energy, and time. The design of this detector is described, and results from the 1987 TFTR run are presented. These results are roughly consistent with predictions from a simple first-orbit particle loss model with respect to the pitch angle, energy, time, and plasma current dependences of the signals.

DISCLAIMER

1. INTRODUCTION

Tokamak ignition with D-T fuel depends upon alpha particle heating, which in turn depends upon good alpha particle confinement. Good alpha particle confinement (e.g, less than 10% alpha loss) is predicted by the classical single-particle model at plasma currents above 3 MA [1]. In this model the alpha losses to the wall are mainly due to the prompt first-orbit loss, while particles confined on their first orbit stay confined until they are thermalized after about 1 sec.

However, if unexpected alpha particle losses are encountered, e.g, due to collective instabilities [1,2], then ignition will be more difficult. Therefore, it seems worthwhile to test the classical single-particle confinement model with presently available alpha-like charged fusion products, namely, the 1 MeV triton and 3 MeV proton created in D-D reactions [3].

This paper describes the behavior of these escaping D-D charged fusion products as measured during operation of TFTR in 1987. These particles are detected just outside the plasma boundary using a new 2-D imaging detector system which can measure flux vs pitch angle, energy, and time, as described in Sec. 2. The results are roughly consistent with the predictions of a classical first-orbit loss model, as described in Sec. 3. The conclusions, including prospects for future measurements along these lines, are given in Sec. 4.

2. DETECTOR DESIGN

The present detector combines the features of two earlier designs. The geometry here is similar to that used in an early PLT experiment [4] which measured D-^{3}He fusion products with a plastic track detector. That design had good

pitch angle resolution and fair energy resolution, but no time resolution, since the plastic had to be removed and examined for individual particle tracks. This difficulty is avoided here by replacing the plastic detector with a ZnS scintillator screen which was optically coupled to a video camera for good time resolution. The ZnS scintillator itself was used in a recent TFTR experiment [5] which measured D-D fusion products, but without pitch angle or energy resolution.

A schematic view of the present detector is shown in Fig. 1. The detection element itself is a 1"x1" ZnS(Ag) scintillator screen mounted inside a light-tight box. This scintillator screen is oriented so that particles which pass through the front "pinhole" and rear "slit" apertures impact the ≈10-15μ ZnS layer, which was coated onto a 1 mm quartz substrate for support. The resulting 2-D image of the scintillation light (450-500 nm) is optically coupled through a relay lens system to a coherent fiber bundle for transmission to a video camera located in a shielded basement.

The pitch angle of the particles χ (i.e, the angle of their gyromotion with respect to the toroidal field B_T) is determined by the angle between the front "pinhole" and the measured impact position as measured along the "pitch angle" coordinate of the scintillator, as shown in Fig. 2(a). The geometrical pitch angle resolution of $\delta\chi \approx \pm 3^\circ$ (FWHM) was determined by the width of the front aperture W=2 mm. The range of detected pitch angles of $\chi \approx 40^\circ$-90° was determined by the orientation of the detector box and apertures, which was centered at $\chi \approx 60^\circ$ with respect to B_T to see the expected classical first-orbit losses (Sec. 3).

The particle energy is inferred through a measurement of its gyroradius, as shown in Fig. 2(b). The gyroradius $\rho \approx$ 4-5 cm was inferred from the particle impact position B through $B^2 \approx 2D\rho + A^2$. The geometrical energy resolution of about ±50% was determined by the height of the apertures H= 1 mm, which, in turn, was determined by the required detector sensitivity. Good energy resolution was considered of secondary importance here, since the Doppler width of ±25% for

beam-target reactions was expected to dominate the energy spectrum.

The sensitivity of the detector was determined by the areas of the front and rear apertures. These areas were made as large as possible, consistent with the desired pitch angle and energy resolution.

Other features of the design were that the vertical distance D=0.4 cm between the aperture center and the scintillator was minimized in order to avoid overheating of the top of the box due to plasma flow (given this aperture location), and that the size of the detector box was constrained by the vacuum port to be ≈2"x2". The direct line-of-sight through the aperture pair was also constrained so as to not intersect the scintillator itself in order to avoid a soft x-ray background [5], setting an upper limit on H. Note also that the effect of the 3μ aluminum foil behind the slit (which was used to block plasma light) was taken into account in evaluating the incident particle energy.

The ultimate time resolution of this system is determined by the decay time of the ZnS(Ag) scintillation process, which is much less than 10μsec [5]. However, for the present experiment the time resolution was set by the video camera framing rate of 16 msec/field, which is still short compared to TFTR time scales of ≈1 sec.

The detector shown in Fig. 1 was mounted on a bellows assembly and inserted vertically from below into the TFTR vessel at R=265 cm, i.e., at the vessel major radius. The radial location of the top of the box was chosen to be r=101.5 cm, i.e., well outside the typical plasma radius of a=80 cm. At this location the apertures were just inside the radius of the local obstacles at the vessel wall, such that the escaping orbits were not obstructed on their way toward the detector. At this location the temperature inside the detector box during TFTR operation, as measured with a thermocouple, was always less than 90° C.

The sensitivity of the system to particle flux at the scintillator was calibrated before installation using an ^{241}Am alpha source. For an expected flux of $\approx 10^8$ tritons/cm^2-sec at the scintillator it was necessary to use an intensified video camera, in part due to the factor-of-10 light attenuation through the ≈7 m plastic fiber bundle. The exposure time per frame was adjustable through gating of the

camera's microchannel plate.

Note that the estimate of particle flux to the scintillator needs to include both the 1 MeV tritons and also a 30-40% contribution from 3 MeV protons, since these two particles are measured together on the scintillator (they have identical gyroradii and orbits in the plasma). The 0.8 MeV ^{3}He particle also created in D-D reactions does not pass through the 3 μ foil. For simplicity, in the following I will often refer to "triton" detection only, but will mean triton and proton detection.

The primary experimental difficulty with this prototype detector was an large unexpected background proportional to the soft x-ray flux emitted from the plasma. This turned out to be due to the 20-40 keV x-ray tail of the $T_e(0)\approx$5-7 KeV thermal plasma center penetrating the carbon box top. This background resulted in a maximum signal-to-background ratio of only about 4, and prevented triton detection above about 1.3 MA. However, since it almost certainly produced a spatially uniform illumination of the scintillator, it could be subtracted out fairly easily. There was also a smaller background proportional to the neutron/gamma flux, which could be subtracted out similarly.

The detector was removed after about four months in TFTR and recalibrated. The optics and foil were intact and the scintillator calibration was unchanged. The only damage to the probe was some minor surface erosion of the carbon armor which was in contact with plasma flow.

3. EXPERIMENTAL RESULTS

The 2-D images of the scintillator light emission were stored on video tape and later digitized. The results were compared with the first-orbit loss model as follows:

(a) Pitch Angle Dependence

In Fig. 3 is an example of data for the light intensity vs. the pitch angle coordinate across the scintillator. In this example the plasma current was I=0.9 MA, the toroidal field was B_T=48 kG, and the data were taken from one video frame exposed for 0.5 msec during the steady state of a typical TFTR discharge. The neutron rate was S=5x10^{15} n/sec, with 12 MW of neutral beam injection (NBI). Here the intensity vs. pitch angle is evaluated at the "gyroradius" dimension correspoding to 1 MeV tritons (averaged over ≈0.4 cm as measured on the scintillator) [see Sec. 3(b)].

This signal should be compared with the "background" curve which was taken during a discharge at 1.4 MA when there was a large soft x-ray flux but no NBI, i.e., no escaping triton flux. This background curve is normalized to the signal curve such that only the difference between these two curves represents the escaping triton flux.

This net triton signal is plotted vs. pitch angle in Fig. 4, including a correction for the variation in optical sensitivity vs. pitch angle (taken from the shape of the background curve). The total pitch angle resolution of the system is about ±4°, due to the finite aperture width W (±3°), the relay lens optics (±2°), and the fiber bundle (±2°). The alignment in pitch angle is accurate to about ±3° (as shown by the error bar).

The expected particle flux vs. pitch angle was calculated using a standard particle orbit code [6,7], with the result as shown in Fig. 4. For 1 MeV tritons (or 3 MeV protons) the expected flux into this detector peaked at $\chi \approx 60°$ (with respect to the direction parallel to the plasma current), a result consistent with previous calculations of escaping alpha flux [1,8,9]. The location of this peak corresponds to the pitch angle of the "fattest banana" orbit which passes closest to high triton source region at the plasma center, as shown in Fig. 5(a). The model curve in Fig. 4 represents the range of expected results over an assumed triton source profile $S(r) \propto [1-(r/a)^2]^{4-8}$ and an assumed plasma current distribution $J(r) \propto [1-(r/a)^2]^{3-5}$.

The result is that the measured pitch angle distribution of escaping 1 MeV triton flux is roughly consistent with expected first-orbit loss, given the pitch angle resolution and alignment uncertainty in this experiment.

b) Energy Dependence

In Fig. 6 are two examples of data for light intensity vs. the "gyroradius" coordinate across the scintillator (this coordinate is approximately $\propto \rho^{1/2}$). Each of these curves is taken from one video frame during the steady state of a 0.9 MA NBI discharge, as for Fig. 2. Two different shots are shown with (a) B_T=48 kG and (b) B_T=28 kG, in order to check the expected effect of B_T on the gyroradius. For both cases the flux is evaluated near the peak of the pitch angle curve of Fig. 2 ($\chi \approx 60\text{-}65^\circ$).

The peak of the light intensity in both cases is near to that expected for 1 MeV tritons, assuming that the gyroradius is proportional to $\cos\chi/B_T$, and taking into account the 25% energy loss of tritons in the aluminum foil (the 3 MeV proton orbits have a slightly larger gyroradius due to relatively lower energy loss).

The broadness of these peaks, about ±0.8 cm FWHM for 48 kG case (at the scintillator), is close to that expected due to the finite aperture height, which allows a single gyroradius spread over $\delta B \approx (\rho/A)H/2 \approx \pm 0.6$ cm in this direction [see Fig. 2(b)]. Additional broadening is due to the triton/proton gyroradius difference (after the foil), to the optical and fiber bundle resolutions, and to the ≈25% Doppler width of 1 MeV tritons.

The result is that the measured gyroradius is roughly consistent with the expected first-orbit loss model, in which the tritons and protons escape with negligible energy loss, at least to within the ±50% energy resolution of the present detector.

(c) Time Dependence

In Fig. 7 is an example of the time dependence of the escaping triton signal vs. the 2.5 MeV neutron (=1 MeV triton) source rate. In this case the triton signal is measured at the peak of the 2-D distribution on the scintillator ($\chi \approx 60\text{-}65^{\circ}$ and $E \approx 1$ MeV), and the time-dependent background has been subtracted out using an area of the scintillator away from possible triton impact. This again was for a 0.9 MA shot with the NBI turned on between 4 and 5 sec.

The escaping triton flux followed the global triton source rate fairly closely in time. The small differences observed between the triton signal and the triton source rate might be due to the 16 msec uncertainty in the camera timing, or the uncertainty in subtracting out the soft x-ray background (particularly after NBI when the soft x-ray background is relatively highest).

The result is that the measured time dependence of the escaping triton flux is roughly consistent with that expected for "prompt" first-orbit loss, which occurs within $<100\mu$sec of creation. Particularly interesting is the absence of non-prompt loss during the period 0.3-0.5 sec after NBI, since the confined triton population is still large at this time, the classical triton slowing-down time being ≈ 1 sec. Note, however, that some differences between the time dependence of the global source and this escaping triton signal are expected due to time-dependent changes in the radial profiles of the triton source and plasma current .

(d) Plasma Current Dependence

In Fig. 8 are some examples of data for the light intensity vs. pitch angle analyzed similarly to Fig. 2, but for shots with plasma currents over the range 0.9-1.3 MA. Each curve was taken from a single video frame at a time when the

neutron rates were identical to within ±10% (at $S=5x10^{15}$n/sec). All were taken on the same day at B_T=48 kG with 12 MW of NBI.

These examples show that the escaping triton flux (per neutron) decreases as the plasma current increases. This trend is plotted for about 20 such shots in Fig. 9, where the escaping triton flux is again evaluated at the peak in pitch angle ($\chi \approx 60\text{-}65^\circ$). Note that the soft x-ray background increases with plasma current, such that the triton signal is hardly distinguishable above background at 1.3 MA.

The expected first-orbit loss vs. plasma current at this pitch angle is also shown in Fig. 9. At higher currents the expected flux is lower because the orbits originate nearer the plasma edge, as shown in Fig. 5(b). The shaded area in Fig. 9 represents the range of variation due to uncertainty in the triton source rate (parabolic exponent 4-8) and current profile (parabolic exponent 3-5). The approximate invariance of the shape of the pitch angle distribution seen in Fig. 8 is also seen in the orbit code predictions.

The result is that the measured plasma current dependence of the escaping triton flux is also roughly consistent with the expected variation of first-orbit losses, at least to within the joint uncertainties of the experiment and model.

(e) Absolute Flux

Up to this point only the relative pitch angle, energy, time, and current dependences of the escaping triton flux were discussed. The absolute triton flux can be estimated based on a benchtop calibration of the system with an ^{241}Am alpha source made with the scintillator plate reversed.

For this estimate an assumption concerning the relative scintillation light intensity for 4.5 MeV alphas (^{241}Am) vs. tritons and protons needs to be made, since no D-D source was available for cross-calibration. As discussed previously[5], if the light emission is assumed proportional to the energy deposited in the scintillator, then the 4.5 MeV alpha produces about four times the light of a 1 MeV

triton, and the 3 MeV proton produces about 30% the light of a 1 MeV triton (this takes into account the attenuation in the foil and penetration distance through the thin ZnS layer). With this assumption, the total triton flux at the scintillator for the 0.9 MA case of Fig. 2 (obtained by integrating over an impact area $\approx$0.6x1.6 cm) is $\approx 2 \times 10^8$ tritons/sec at a neutron flux of 3×10^{15} n/s. This estimate of triton flux is uncertain by at least a factor of 2-3, due to the assumed scintillator response to protons and tritons, to the uncertainties in the ^{214}Am calibration itself, and to the difficulty of integrating the measured triton flux over the scintillator area in the presence of the large soft-x-ray background.

The expected triton flux incident on the scintillator for this case was calculated using the orbit code, which models the flux through a pair of apertures similar to those in this experiment. The results were in the range $\approx 3 \times 10^8$ triton/sec at an assumed neutron rate of 3×10^{15} n/s, with about a factor of 2 variation due to the range of possible source and current profiles. With the additional uncertainties in the neutron source rate calibration and in the aperture modelling, the net result is uncertain by at least a factor of 3.

The tentative result is that the measured escaping triton flux is again roughly consistent with the predicted first-orbit loss, but only to within the large joint uncertainties.

4. CONCLUSIONS

This paper reported the pitch angle, energy, and time-dependent behavior of escaping D-D fusion products in TFTR as measured with a new type of imaging detector. The results were consistent in many respects with the expected classical first-orbit loss model. In particular, the predicted peak in the flux vs. pitch angle (Fig. 4) and decrease in flux with increased plasma current (Fig. 9) were measured

clearly for the first time in tokamaks. The apparent absence of non-prompt loss was also seen in the time dependence of the triton signal, particularly after NBI (Fig. 7).

The prototype detector system described in Sec. 2 worked successfully, but could be improved at several points. Most important, and quite simple, would be an improvement in soft x-ray shielding above the scintillator (e.g., 3 mm iron), which would eliminate the largest background and so allow clean measurement of the high frequency components of the signal. Also useful would be replacement of the plastic coherent fiber bundle with lower-loss, radiation resistant quartz fibers.

Although the present results are consistent with the trends predicted by the simple prompt-loss model, it is difficult at this point to exclude the possible influence of toroidal field (or MHD-induced) ripple [10,11], since these effects tend to produce the same relative trends as the prompt-loss model. For example, stochastic diffusion in the toroidal field ripple tends to broaden the effective triton source profile on a fast (<100 msec) time-scale, and so would be difficult to distinguish from first-orbit loss from a broader radial profile, at least without an accurate absolute calibration. Future experiments might try to change the effective ripple to resolve this effect, e.g., through radial plasma movement. Also useful in this regard would be a poloidal/toroidal array of detectors, e.g., since the stochastic ripple losses tend to occur more toward the outer equator than prompt losses.

The detector described here can also be used with D-T-generated escaping 3.5 MeV alpha particles which have nearly the same gyroradius as 1 MeV tritons or 3 MeV protons. In that case the dominant background should be the relatively small neutron or gamma interactions with the scintillator itself [5]. If so, then the $\approx$100 times larger signals with D-T alphas should allow improved energy and/or pitch angle resolution, since the aperture height and/or width could be reduced.

ACKNOWLEDGMENTS

Particular thanks go to J. D. Strachan and K. M. Young for supporting and encouraging this project, and to T. Deverell for help with its construction. Thanks also to F. Dylla, K. Hill, D. Johnson, L. Johnson, P. LaMarche, D. Manos, K. Owens, and M. Ulrickson of PPPL for advice on the detector design. This work was supported under U.S. Department of Energy Contract No. DE-AC02-76-CHO3073.

REFERENCES

[1] Kolesnichenko, Y. I., Nucl. Fusion 20 (1980) 727.

[2] Zweben, S.J., Furth, H.P., Mikkelsen, D.R., Redi, M.H., and Strachan, J.D., Princeton Plasma Physics Lab Report PPPL-2535, "Alpha Storage Regime in High Temperature Sub-Ignited D-T Plasmas," 1988 (to be published in Nucl. Fusion).

[3] Zweben, S.J., Physica Scripta T16 (1987) 119.

[4] Murphy, T.J. and Strachan, J.D., Nucl. Fusion 25 (1985) 383.

[5] Zweben, S.J., Princeton Plasma Physics Lab Report PPPL-2559, "Four-Channel ZnS Scintillator Measurements of Escaping Tritons in TFTR," 1988 (to be published in Rev. Sci. Instrum.)

[6] R.E. Chrien and J.D. Strachan, Phys. Fluids 26 (1983) 1953.

[7] W.W. Heidbrink and J.D. Strachan, Rev. Sci. Instrum. 56 (1985) 501.

[8] Hively, L.M. and Miley, G.H., Nucl. Fusion 17 (1977) 1031.

[9] Bauer, W., Wilson, K.L., Bisson, C.L., and Goldston, R.J., Nucl. Fusion 19 (1979) 93.

[10] Tani, K., Takizuka, T., Azumi, M., Kishimoto, H., Nucl. Fusion 23 (1983) 657.

[11] White, R.B. and Mynick, H.E., Princeton Plasma Physics Lab Report PPPL-2563, "Alpha Particle Confinement in Tokamaks," 1988.

FIGURE CAPTIONS

1) Schematic views of the detector. The scintillator is mounted at the end of a probe inserted into the bottom of the TFTR vacuum vessel. The charged fusion products are dispersed according to pitch angle along one dimension of the scintillator and according to gyroradius (i.e., energy) along the other (in orthogonal polar coordinates). The 2-D scintillator image is optically coupled to a video camera and VCR.

2) Details showing the detector geometry for measuring (a) pitch angle and (b) energy. The pitch angle is determined by the angle between the particle impact position and the front pinhole, with an angular resolution set by the front aperture width. The energy is determined from the impact position B with a resolution set by the aperture height H. Here $A \approx 0.5$ cm, $B \approx 2$ cm, $C \approx 3.5$ cm, $D \approx 0.4$ cm, $H \approx 0.1$ cm, and $W \approx 0.2$ cm. The design also ensures that the direct line-of-sight through the apertures misses the scintillator at C.

3) Example of data for the scintillator light intensity vs. pitch angle as measured at a gyroradius corresponding to 1 MeV tritons (or 3 MeV protons). The signal curve was taken from one video frame exposed for 0.5 msec at a neutron (triton) source rate of 5×10^{15} n/sec. The background frame was taken during an ohmic plasma when the neutron rate was negligible but the soft x-ray flux was high. The difference between these two curves (normalized at $\chi \approx 50^{\circ}$) represents the triton signal.

4) Measurement vs. model prediction for flux vs. pitch angle for 1 MeV tritons. The experimental curve comes from Fig. 2 after background subtraction and optical sensitivity correction. The model curve comes from the particle orbit code and represents the range of plausible radial source and current profiles. The two curves agree to within the joint uncertainties, including an $\approx 3^{\circ}$ angular alignment

uncertainty shown by the error bar. Note that only the relative shapes of the flux vs. pitch angle are plotted here [the absolute flux comparison is discussed in Sec III(e)].

5) Orbit code results showing typical 1 MeV triton trajectories expected for different (a) pitch angles and (b) plasma currents. All orbits are constrained to go through the detector. In (a) the plasma current is 0.9 MA and in (b) the pitch angle is 62°.

6) Example of data for light intensity vs. the "gyroradius" coordinate as measured at a pitch angle of $\chi \approx 60\text{-}65°$ for two different toroidal fields. The "gyroradius" coordinate B is approximately proportional to $\rho^{1/2}$, as shown in Fig. 2. In both cases the peak signal lies near to the position on the scintillator expected for 1 MeV tritons (right edge of shaded region) or 3 MeV protons (left edge of shaded region). The expected shift in the peak due to $\rho \propto B^{-1}$ is observed. The large width of these curves is expected due to the finite aperture height.

7) Measured time dependence of the triton signal evaluated at a pitch angle of $\chi \approx 60\text{-}65°$ and a triton energy $E \approx 1$ MeV. The escaping triton signal roughly follows the triton source rate as monitored by the 2.5 MeV neutron flux, as expected from the prompt first-orbit loss model. Note that there is a slight detector saturation at the peak of the triton signal which causes those points to be somewhat low.

8) Examples of the measured light intensity vs. pitch angle similar to Fig. 2, but for plasma currents 0.9-1.3 MA. These signals are all taken at a neutron rate of 5×10^{15} n/sec and a gyroradius corresponding to 1 MeV tritons. The net triton signal decreases as the plasma current increases, until at 1.3 MA the triton signal is hardly observable above the soft x-ray noise level (which increases with plasma current). The shape of the background curve is taken from a 1.4 MA ohmic discharge with no escaping tritons.

9) Escaping triton flux per neutron vs. plasma current, evaluated at a pitch angle

of $\chi \approx 60\text{-}65^{\circ}$ and a triton energy of $E \approx 1$ MeV. The experimental points come from a series of shots like those shown in Fig. 8 (after background subtraction). The first-orbit model represents the same range of profile assumptions used for Fig. 4. The measured decrease in escaping triton flux with increased plasma current is roughly consistent with the model. The error bar indicates approximate shot-to-shot variation.

#88X1129

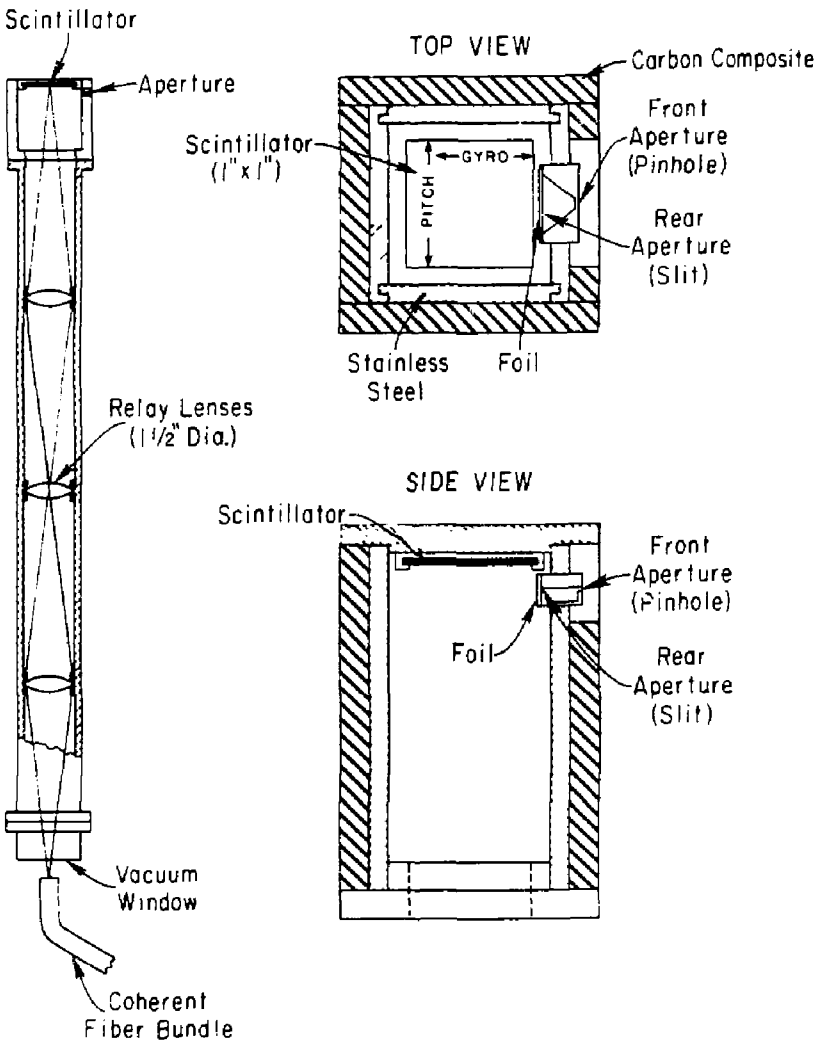

Fig. 1

#88X1132

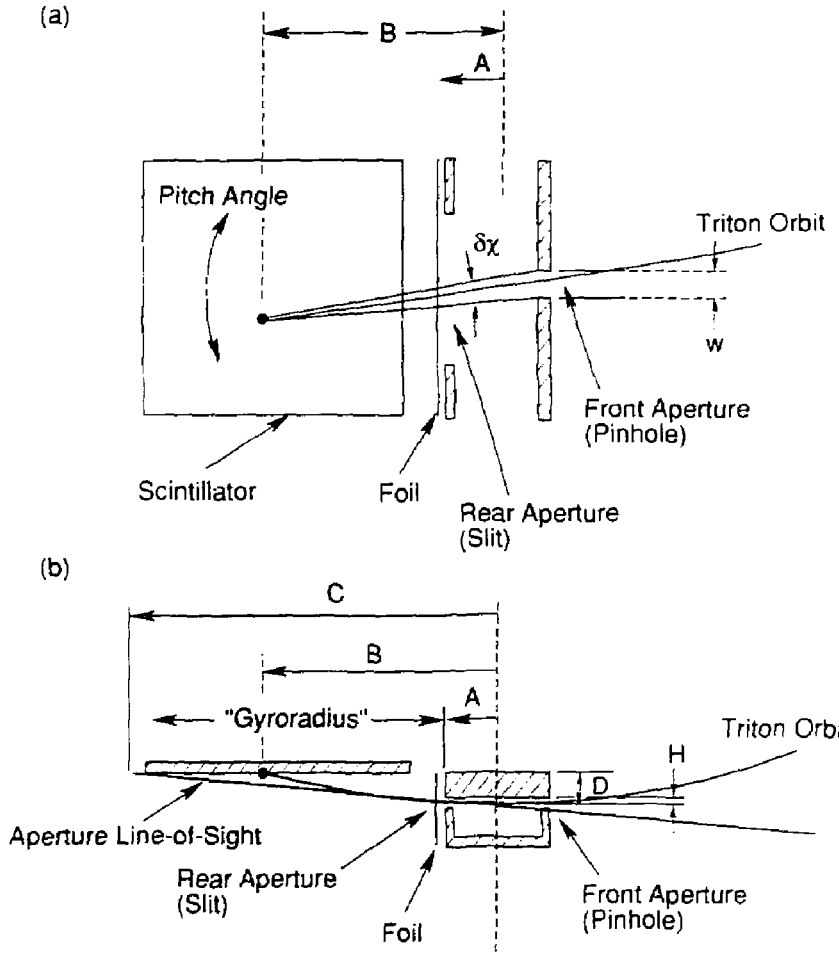

Fig. 2

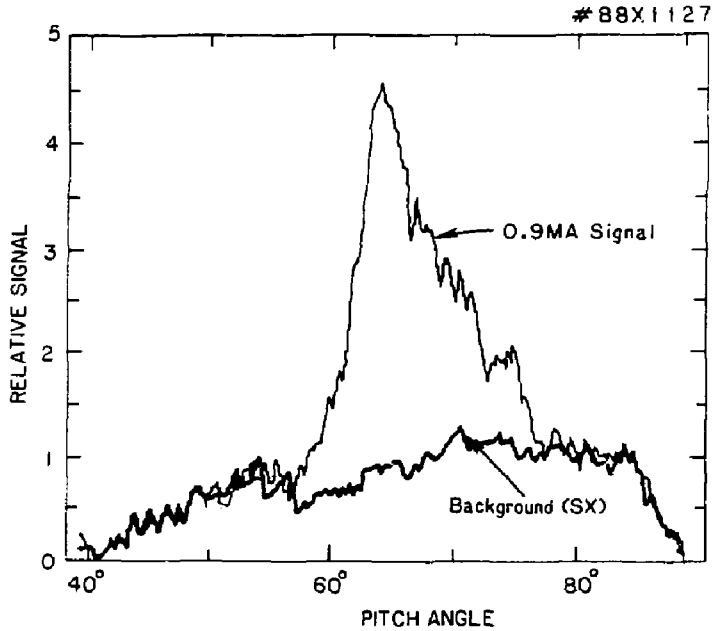
#88X1127
RELATIVE SIGNAL
0
1
2
3
4
5
40°
60°
80°
PITCH ANGLE
0.9MA Signal
Background (SX)

Fig. 3

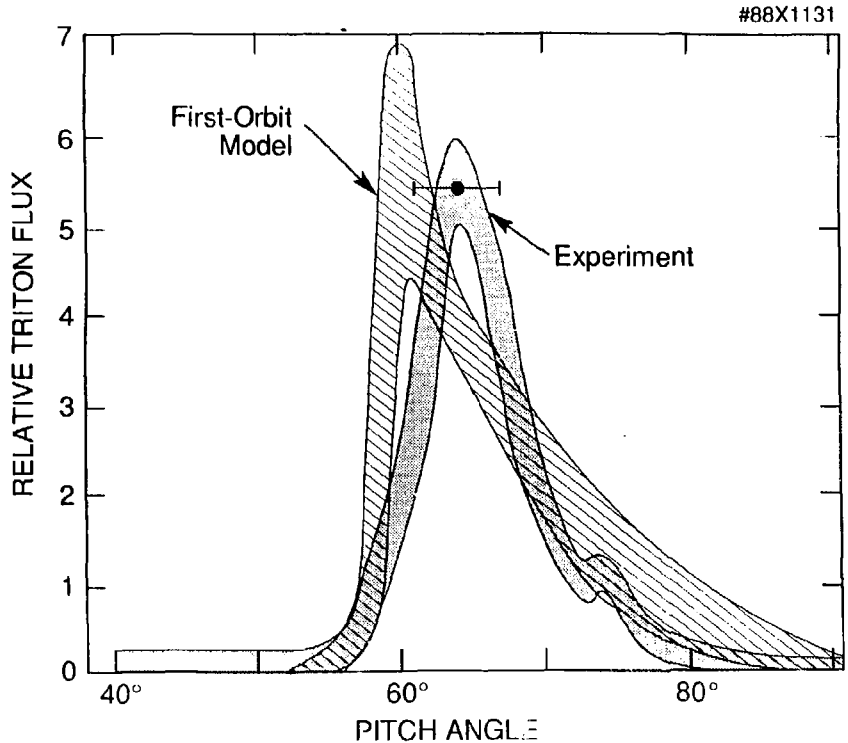
#88X1131
First-Orbit
Model
Experiment
RELATIVE TRITON FLUX
0
1
2
3
4
5
6
7
40°
60°
80°
PITCH ANGLE

FIG. 4

#88X1135

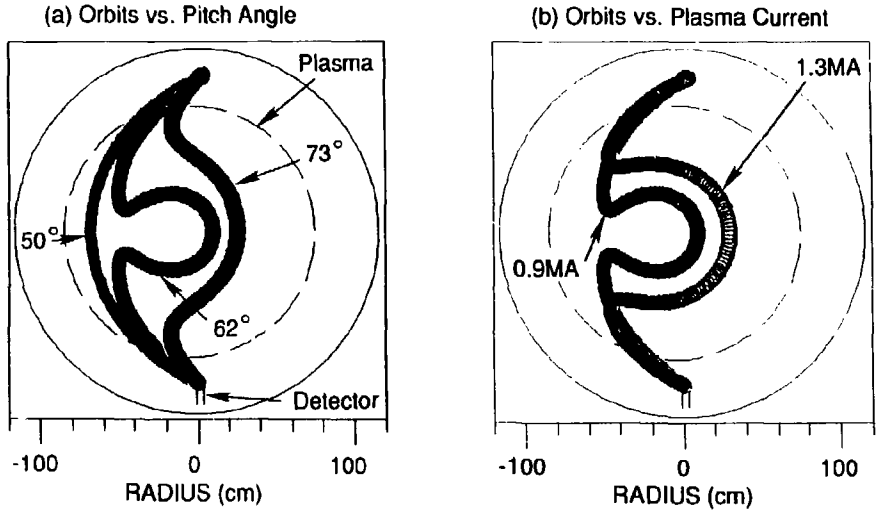

Fig. 5

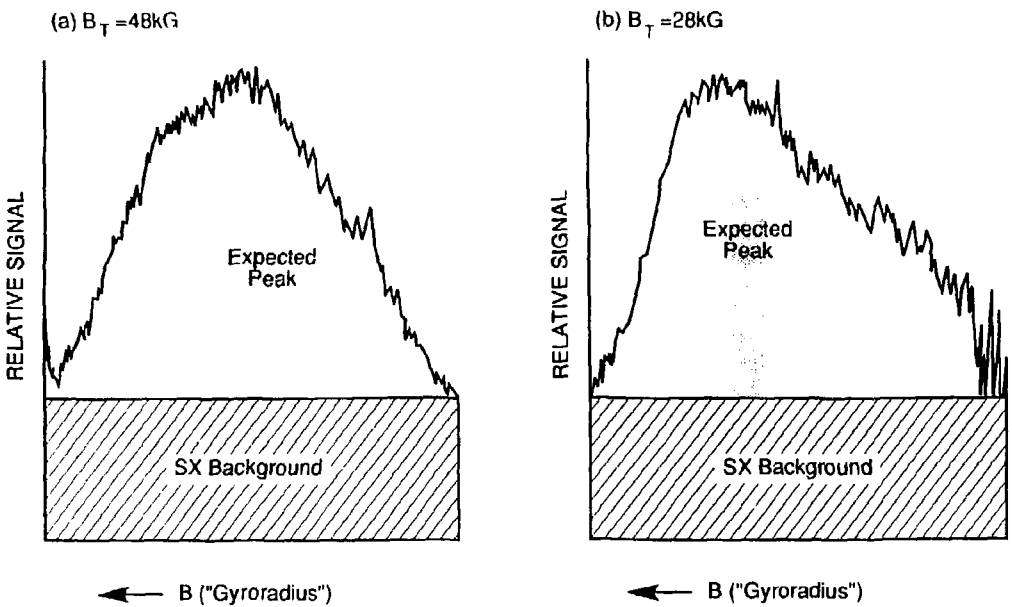
(a) B_T =48kG
RELATIVE SIGNAL
Expected Peak
SX Background
B ("Gyroradius")
(b) B_T =28kG
RELATIVE SIGNAL
Expected Peak
SX Background
B ("Gyroradius")

Fig. 6

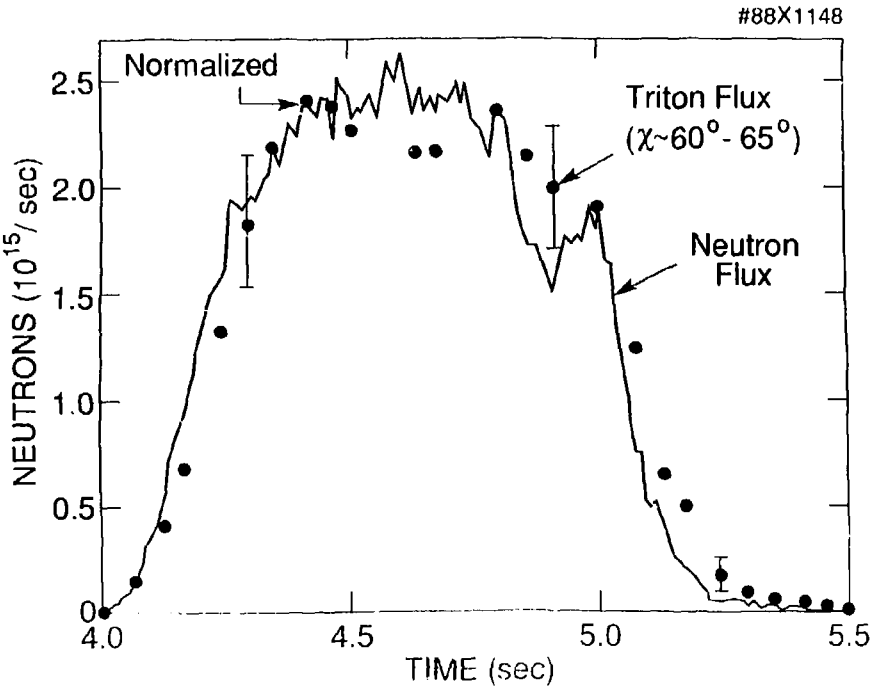
#88X1148
Normalized
Triton Flux
(χ~60°- 65°)
Neutron
Flux
NEUTRONS (10^15/ sec)
2.5
2.0
1.5
1.0
0.5
0
4.0
4.5
5.0
5.5
TIME (sec)

Fig. 7

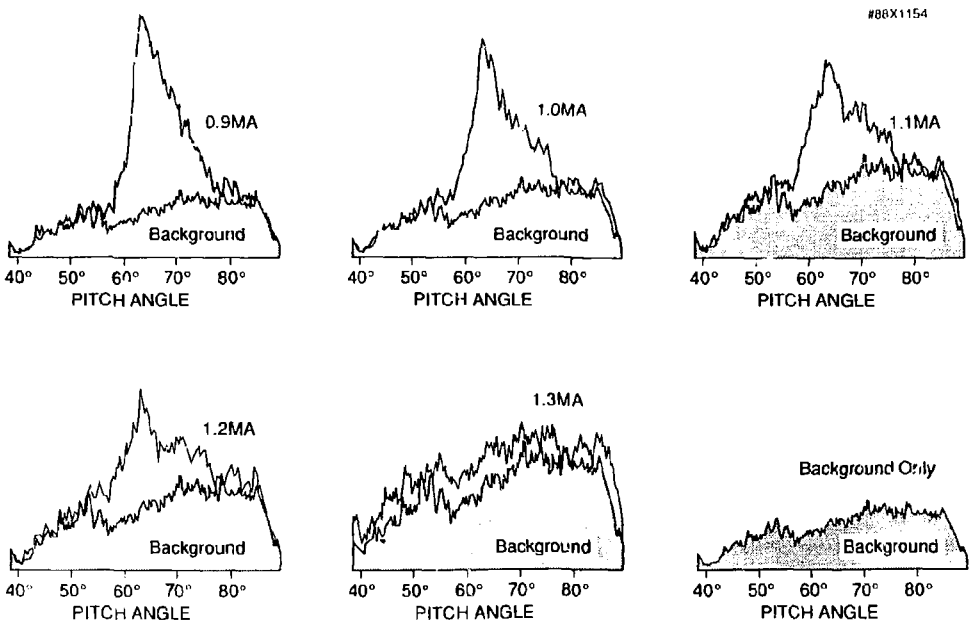
#88X1154
0.9MA
Background
40° 50° 60° 70° 80°
PITCH ANGLE
1.0MA
Background
40° 50° 60° 70° 80°
PITCH ANGLE
1.1MA
Background
40° 50° 60° 70° 80°
PITCH ANGLE
1.2MA
Background
40° 50° 60° 70° 80°
PITCH ANGLE
1.3MA
Background
40° 50° 60° 70° 80°
PITCH ANGLE
Background Only
Background
40° 50° 60° 70° 80°
PITCH ANGLE

Fig. 8

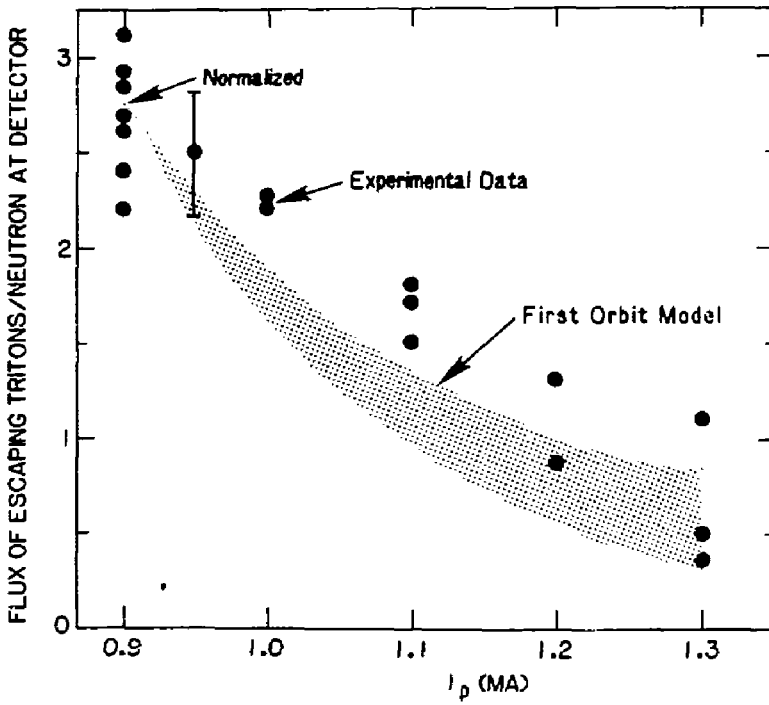
FLUX OF ESCAPING TRITONS/NEUTRON AT DETECTOR
3
2
1
0
Normalized
Experimental Data
First Orbit Model
0.9
1.0
1.1
1.2
1.3
I_p (MA)

Fig. 9

EXTERNAL DISTRIBUTION IN ADDITION TO UC-20

Dr. Frank J. Paoloni, Univ of Wollongong, AUSTRALIA
Prof. M.H. Brennan, Univ Sydney, AUSTRALIA
Plasma Research Lab., Australian Nat. Univ., AUSTRALIA
Prof. I.R. Jones, Flinders Univ., AUSTRALIA
Prof. F. Cap, Inst Theo Phys, AUSTRIA
Prof. M. Heindler, Institut fur Theoretische Physik, AUSTRIA
M. Goossens, Astronomisch Instituut, BELGIUM
Ecole Royale Militaire, Lab de Phys Plasmas, BELGIUM
Commission-European, Dg-XII Fusion Prog, BELGIUM
Prof. R. Boucique, Laboratorium voor Natuurkunde, BELGIUM
Dr. P.H. Sakanaka, Instituto Fisica, BRAZIL
Instituto De Pesquisas Espaciasi-INPE, BRAZIL
Documents Office, Atomic Energy of Canada Limited, CANADA
Dr. M.P. Bachynski, MPB Technologies, Inc., CANADA
Dr. H.M. Skarsgard, University of Saskatchewan, CANADA
Dr. H. Barnard, University of British Columbia, CANADA
Prof. J. Teichmann, Univ. of Montreal, CANADA
Prof. S.R. Sreenivasan, University of Calgary, CANADA
Prof. Tudor W. Johnston, INRS-Energie, CANADA
Dr. C.R. James, Univ. of Alberta, CANADA
Dr. Peter Lukac, Komenskeho Univ, CZECHOSLOVAKIA
The Librarian, Culham Laboratory, ENGLAND
The Librarian, Rutherford Appleton Laboratory, ENGLAND
Mrs. S.A. Hutchinson, JET Library, ENGLAND
C. Mouttet, Lab. de Physique des Milieux Ionises, FRANCE
J. Radet, CEN/CADARACHE - Bat 506, FRANCE
Univ. of Ioannina, Library of Physics Dept. GREECE
Dr. Tom Mual, Academy Bibliographic Ser., HONG KONG
Preprint Library, Hungarian Academy of Sciences, HUNGARY
Dr. B. Dasgupta, Saha Inst of Nucl. Phys., INDIA
Dr. P. Kaw, Institute for Plasma Research, INDIA
Dr. Philip Rosenau, Israel Inst. Tech, ISRAEL
Librarian, Int'l Ctr Theo Phys, ITALY
Prof. G. Rostagni, Univ Di Padova, ITALY
Miss Clelia De Palo, Assoc EURATOM-ENEA, ITALY
Biblioteca, Instituto di Fisica del Plasma, ITALY
Dr. H. Yamato, Toshiba Res & Dev, JAPAN
Prof. I. Kawakami, Atomic Energy Res. Institute, JAPAN
Prof. Kyoji Nishikawa, Univ of Hiroshima, JAPAN
Direc. Dept. Large Tokamak Res. JAERI, JAPAN
Prof. Satoshi Itoh, Kyushu University, JAPAN
Research Info Center, Nagoya University, JAPAN
Prof. S. Tanaka, Kyoto University, JAPAN
Library, Kyoto University, JAPAN
Prof. Nobuyuki Inoue, University of Tokyo, JAPAN
S. Mori, JAERI, JAPAN
Librarian, Korea Advanced Energy Res. Institute, KOREA
Prof. D.I. Choi, Adv. Inst Sci & Tech, KOREA
Prof. B.S. Liley, University of Waikato, NEW ZEALAND
Institute of Plasma Physics, PEOPLE'S REPUBLIC OF CHINA
Librarian, Institute of Phys., PEOPLE'S REPUBLIC OF CHINA
Library, Tsing Hua University, PEOPLE'S REPUBLIC OF CHINA
Z. Li, Southwest Inst. Physics, PEOPLE'S REPUBLIC OF CHINA
Prof. J.A.C. Cabral, Inst Superior Tecnico, PORTUGAL
Dr. Octavian Petrus, AL I CUZA University, ROMANIA
Dr. Johan de Villiers, Fusion Studies, AEC, SO AFRICA
Prof. M.A. Hellberg, University of Natal, SO AFRICA
C.I.E.M.A.T., Fusion Div. Library, SPAIN
Dr. Lennart Stenflo, University of UMEA, SWEDEN
Library, Royal Inst Tech, SWEDEN
Prof. Hans Wilhelmson, Chalmers Univ Tech, SWEDEN
Centre Phys des Plasmas, Ecole Polytech Fed, SWITZERLAND
Bibliotheek, Fom-Inst Voor Plasma-Fysica, THE NETHERLANDS
Dr. O.D. Ryutov, Siberian Acad Sci, USSR
Dr. G.A. Eliseev, Kurchatov Institute, USSR
Dr. V.A. Glukhikh, Inst Electrophysical Apparatus, USSR
Dr. V.T. Tolok, Inst. Phys. Tech. USSR
Dr. L.M. Kovrizhnykh, Institute Gen. Physics, USSR
Nuclear Res. Establishment, Julich Ltd., W. GERMANY
Bibliothek, Inst. Fur Plasmaforschung, W. GERMANY
Dr. K. Schindler, Ruhr Universitat Bochum, W. GERMANY
ASDEX Reading Rm, IPP/Max-Planck-Institut fur Plasmaphysik, W. GERMANY
Librarian, Max-Planck Institut, W. GERMANY
Prof. R.K. Janev, Inst Phys, YUGOSLAVIA